HHS Public Access

Author manuscript

NMR Biomed. Author manuscript; available in PMC 2017 February 01.

Published in final edited form as:

NMR Biomed. 2016 February ; 29(2): 187–196. doi:10.1002/nbm.3265.

Sodium MRI in human heart: a review

Paul A Bottomley

Division of MR Research, Department of Radiology, Park Bldg 310, Johns Hopkins University, 601 600 N, Caroline Wolfe Street, Baltimore MD, USA 21287-0843, PH: (USA) 410 955 0366, FAX: (USA) 410 614 1977, bottoml@mri.jhu.edu

Abstract

This paper offers a critical review of the properties, methods and potential clinical application of sodium (^{23}Na) magnetic resonance imaging (MRI) in human heart. Because the tissue sodium concentration (TSC) in heart is about ~40μmol/g wet wt, and the ^{23}Na gyromagnetic ratio and sensitivity are respectively about 1/4th and 1/11th that of hydrogen (^{1}H), the signal-to-noise ratio of ^{23}Na MRI in heart is about 1/6000th that of conventional cardiac ^{1}H MRI. In addition, as a quadrupolar nucleus, ^{23}Na exhibits ultra-short and multi-component relaxation behavior (T_1~30ms; T_2 ~0.5–4ms and 12–20ms), that requires fast, specialized, ultra-short echo-time MRI sequences, especially for quantifying TSC. Cardiac ^{23}Na MRI studies from 1.5–7 T measure a volume-weighted sum of intra- and extra-cellular components present at cytosolic concentrations of 10–15 mM and 135–150 mM in healthy tissue, respectively, at a spatial resolution of about 0.1–1 ml in 10 min or so. Presently, intra- and extra-cellular sodium cannot be unambiguously resolved without the use of potentially toxic shift reagents. Nevertheless, increases in TSC attributable to an influx of intra-cellular sodium and/or increased extra-cellular volume have been demonstrated in human myocardial infarction consistent with prior animal studies, and arguably might also be seen in future studies of ischemia, and cardiomyopathies–especially those involving defects in sodium transport. While technical implementation remains a hurdle, a central question for clinical use is whether cardiac ^{23}Na MRI can deliver useful information unobtainable by other more convenient methods, including ^{1}H MRI.

Graphical abstract

The properties, methods and clinical potential of sodium MRI in human heart are reviewed. The myocardial sodium concentration is about ~40μmol/g.wet.wt., and its signal-to-noise ratio is about 1/6000th of conventional proton MRI. Sodium's short multi-component relaxation behavior necessitates fast, ultra-short-echo MRI sequences, especially for quantification. Presently, intra- and extra-cellular sodium cannot be unambiguously resolved, but increased sodium primarily attributable to sodium influx, is demonstrated in human myocardial infarction. The added value of cardiac ^{23}Na MRI vs. existing methods remains key.

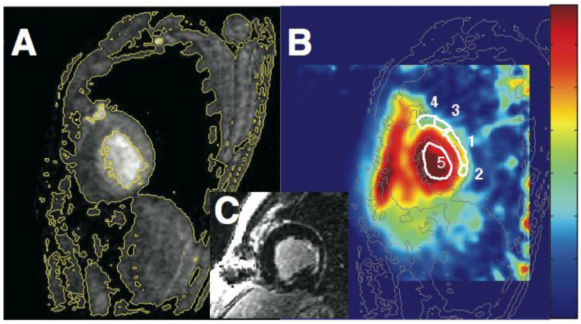

Keywords

heart; sodium; magnetic resonance imaging (MRI); ultra-short echo-time; T_1; T_2; quantification; total sodium content; myocardial infarction

INTRODUCTION

Sodium plays a vital role in myocyte function and integrity. The sodium concentration is 8–10 times higher in the extracellular vs. the intracellular space, with the trans-membrane sodium flux and osmotic balance regulated by the sodium-potassium pump. The sodium channel mediates the rapid upbeat of the cardiac action potential and calcium exchange, which are critical to cardiac excitability, conduction and muscular contraction (1–4). Alterations in tissue sodium concentration (TSC) and in trans-membrane sodium flux occur in ischemic heart disease and myocardial infarction (MI)(5,6). Sodium channel dysfunction is also linked to dilated and hypertrophic cardiomyopathies (7–12). While serum sodium levels are routinely measured in patients and may be independent predictors of outcome for certain heart failure etiologies (11), these measures can only detect electrolyte imbalances that affect the entire blood pool. Except for sodium (^{23}Na) magnetic resonance imaging (MRI), direct *in vivo* sampling of cardiac sodium is only possible via myocardial biopsy during cardiac surgery or image-guided intervention undertaken for other purposes (12). This makes ^{23}Na MRI a uniquely noninvasive tool for accessing myocardial sodium *in vivo*.

PROPERTIES

Signal-to-noise ratio (SNR)

Fifty years have passed since the first ^{23}Na nuclear magnetic resonance (MR) studies of sodium in muscle (13). ^{23}Na MRI of isolated rodent hearts (14), and the first human cardiac ^{23}Na MRI (15,16) were reported in the 1980s following the innovation of 1.5 T whole-body scanners, which provided the requisite signal-to-noise ratio (SNR) unavailable to early 0.04–0.3 T scanners (17). Indeed, after accounting for the myocardial sodium tissue concentration of ~40 mmol/kg wet weight, the lower ^{23}Na MR sensitivity and gyromagnetic ratio (©) of about 1/4th that of ^{1}H, the SNR of ^{23}Na MRI is some 6000 times lower than that of conventional cardiac proton (^{1}H) MRI under optimum but equivalent detection conditions for both nuclei (Table 1, bottom row). Overcoming this severe, intrinsic SNR handicap to perform ^{23}Na MRI, demands considerable effort.

Optimized detectors, and front-end scanner electronics are certainly essential for ^{23}Na MRI: they are already near-optimal for ^{1}H MRI. Field strength (B_0) is important, but the increase in SNR anticipated from higher B_0 is at best only linear in B_0, assuming that all detectors satisfy the condition that coil noise is negligible compared to sample noise (18). Adjusting the ^{23}Na MRI operating parameters, on the other hand, can have far greater impact. Reducing spatial resolution from 0.5×0.5×3 mm (0.0075 ml)–typical for a ^{1}H MRI study–to 5×5×10 mm or 0.25 ml for ^{23}Na MRI, for example, yields a 333-fold increase in SNR, which can cut the SNR deficit from 6000 to just 18. Being able to image sodium, the prime mover in cellular ion transport, at sub-milliliter resolution by ^{23}Na MRI, is by no means unattractive.

No formal experimental comparison of the B_0-dependence of ^{23}Na SNR under equivalent conditions yet exists, but published ^{23}Na images of human heart acquired at 1.5 T (19–22), 3 T (23–25) and 7 T (26,27) clearly benefit from the huge SNR advantage gained by cutting spatial resolution compared to ^{1}H MRI. Of the most recent human cardiac data, ^{23}Na SNRs of 11–24 are reported in the septum at 3T with a resolution of 4×4×10 mm at 3 T in ~9 min acquisitions (25). Sodium images acquired from heart patients in ~12 min at 1.5 T had 6 mm isotropic resolution, permitting myocardial TSC measurements with an accuracy of ~10% in control subjects (22). The 7T results suggest a SNR of ~24 with 5×5×40 mm resolution in 11 min acquisitions (26), and 10-phase cardiac cine ^{3}Na MRI with 6mm isotropic revolution in ~19 min (27).

Thus, much of the remaining SNR deficit for ^{23}Na–that factor of 18 compared to ^{1}H MRI–is dealt with by signal averaging for 10 minutes or so, as compared to the seconds typically required for ^{1}H MRI with comparable SNR per pixel. The ability to accommodate many averages in practical scan times–the acquisition efficiency–depends critically on the tissue ^{23}Na spin-lattice (T_1) and spin-spin (T_2) relaxation times.

Relaxation times

Initially, it was thought that only 30%–40% of the total tissue sodium was MR-visible (13,28) due to nuclear quadrupolar interactions of this spin-3/2 nucleus (29), and/or interactions with tissue macromolecules. In fact, ^{23}Na commonly exhibits multi-exponential T_2 relaxation in intact biological tissue, with fast (T_{2f}) and slow (T_{2s}) spin-spin relaxation times (30). The T_{2f} component comprises about 40% of the total ^{23}Na signal depending on tissue type (30,31), and is attributable on theoretical grounds, to the motion-averaged electrostatic field gradients arising from reorienting water molecules and charged sites on macromolecules in the vicinity of the ions (29, 32). Experimental data showing a T_{2s} component representing 68±15% of the sodium signal in muscle (32), isolated perfused rat hearts, frog hearts (33), and canine hearts studied *in vivo* (34), is consistent with this theory. In healthy skeletal and cardiac muscle T_{2f} falls in the range 0.5–4 ms, while T_{2s} is 12–32 ms and contributes 68±15% of the total ^{23}Na heart signal (6,24,34–37). Consequently, a major portion of the T_{2f} signal component is lost when spin-echo or gradient-echo times (TE) are longer than about 3 ms. This signal loss and the effect of short T_2s on the useful signal bandwidth (BW), reduces SNR and confounds quantification of absolute TSC. Nevertheless, TSC measured by short-TE ^{23}Na MRI, appears to match tissue [Na] measured by assay (34).

On the plus side, the factors responsible for short ^{23}Na T_2s also produce short T_1 relaxation times of around 10–40 ms (34,35). This means that MRI experiments performed with pulse sequence repetition times TR~60 ms, are essentially fully-relaxed. Some published ^{23}Na MR T_1 and T_2 relaxation times for tissues encountered in the chest and heart are summarized in Table 2 (6, 24, 28, 32–45).

Because ^{23}Na T_1s are about 1/25th of the typical proton (^{1}H) T_1s, ^{23}Na experiments can potentially be conducted ~25 times faster than a conventional ^{1}H study for the same MR saturation level. This should result in a gain in SNR efficiency of about √25 ~5. If in addition the BW is cut 4-fold vs. ^{1}H (compromise to the detection of the T_{2f} component, notwithstanding), the combined effect reduces the residual SNR deficit by √(25×4) =10-fold, from 18 to about 2 (46).

Intra- and extra-cellular sodium

The total tissue sodium concentration, $[Na]_{tissue}$, is a composite of the disparate intra- and extra-cellular sodium concentrations, $[Na]_{intra}$ and $[Na]_{extra}$ (34):

$$[\mathrm{Na}]_{\mathrm{tissue}}^{\mathrm{mmol/kg}} = \left(V_{\mathrm{intra}}[\mathrm{Na}]_{\mathrm{intra}}^{\mathrm{mM}} + V_{\mathrm{extra}}[\mathrm{Na}]_{\mathrm{extra}}^{\mathrm{mmol/kg}}\right) W^{l/\mathrm{kg}} \quad [1]$$

Here $[Na]_{intra}$ is typically 10–15 mM and $[Na]_{extra}$ is 135–150 mM in the cytosol. The V's are the corresponding tissue volume fractions with V_{extra} =1- V_{intra}, and W (in liters/kg or ml/g wet weight) is the tissue water content.

As an example, V_{intra} occupies about 75% of the water space of cardiac tissue (6,47,48), which in turn is about 77% water (6, 49). Thus, use of Eq. [1] yields a tissue TSC of 0.77× (0.75×15+0.25×145) =37 μmol/g wet weight. This excludes contributions from intravascular blood which occupies 8–10% (50) of the tissue but carries a TSC of ~84 μmol/g (38). If a separate 9% intravascular blood component is accounted for, $[Na]_{tissue}$ increases to (37+0.09×84)/1.09 =41 μmol/g, consistent with a measured value of 43 μmol/g for human heart (21).

Ordinarily, the naturally abundant ^{23}Na resonance is a singlet in biological tissue, and $[Na]_{intra}$ and $[Na]_{extra}$ are not resolvable by ^{23}Na NMR. However, introducing a chemical shift reagent such as dysprosium or thulium into the extra-cellular space can peel off the extra-cellular pool into a separate resonance (51,52), resulting in two resonances–one for each. ^{23}Na NMR spectroscopy can then be used to study ion transport between the two pools, for example, under normal and ischemic conditions (52). Unfortunately, these heavy-metal shift reagents are ultimately toxic and unsuitable for human or non-terminal animal studies in their present form.

Note that the mere existence of dual-component ^{23}Na T_2 values has long fueled speculation that each T_2 component might be separately assigned to $[Na]_{intra}$ and $[Na]_{extra}$ (53,54). The hypothesis that each or either T_2 component can be wholly assigned to intra- or extra-cellular sodium is presently unproven. Moreover, there is some evidence against it. This includes ^{23}Na studies of frog heart that show that when the intracellular sodium signal determined from shift reagent experiments, is subtracted from the total signal, the remaining

extra-cellular interstitial sodium remains biexponential with the same T_2s (T_{2f}≈1–2ms and T_{2s}≈17ms; 33). Hence the conclusion that the extra-cellular "*interstitium contains sodium relaxation times that are similar to the relaxation times found for intracellular sodium*" (33). Similarly, studies of fresh rat skeletal muscle up to 24 hrs post-biopsy elicited no significant differences in relaxation components despite equalization of the intra- and extra-cellular sodium concentrations (32). The conclusion was that muscle sodium is "*satisfactorily described as distributed in a single compartment*" from the NMR standpoint (32). While frog heart and rat muscle are not mammalian heart muscle, observations that *neither T_{2f} and T_{2s} nor their relative fractions change* in acute reperfused MI vs. healthy canine myocardium measured *in vivo* despite a doubling of $[Na]_{tissue}$, are consistent with the same conclusion (34). Thus, from the NMR standpoint, it seems that the view from the Na^+ ion is somewhat similar from inside the cell, as it is from the outside.

This is not to say that $[Na]_{intra}$, $[Na]_{extra}$, or T_{2f}, and T_{2s} and their relative fractions can never change under various stresses or disease states. Changes in TSC (or $[Na]_{tissue}$) in response to stress, ischemic disease, infarction, disorders affecting ion transport, therapeutic intervention due to ion pump failure, increased membrane permeability, and/or cell rupture will generally reflect changes in $[Na]_{intra}$, if $[Na]_{extra}$, is maintained in homeostasis by the blood pool. Changes in cellular volume V_{intra}, or vascular volume, due to edema, injury or even exercise would also affect TSC. While this renders ^{23}Na MR sensitive to many cellular level disturbances, it also means that measurements of $[Na]_{tissue}$ alone may not permit resolution of those contributory factors in Eq. [1] that may be causal.

There is hope that newer triple-quantum filtered (TQF) ^{23}Na MRI techniques might help distinguish intra- and extra-cellular cardiac sodium pools, but as in the case of T_{2f} and T_{2s}, support for a hypothesis that it could provide unambiguous resolution of $[Na]_{intra}$ and $[Na]_{extra}$ is presently lacking. Since there are presently no human cardiac TQF ^{23}Na data, we will not address this here.

METHODS

^{23}Na MRI pulse sequence

Table 2 shows that the ^{23}Na tissue MR signal can have multiple contributing T_2 components ranging from 0.5 to 33 ms. It is unclear to what extent the scatter in these values reflect real physiological variability, or just the difficulty and error in measuring them by ^{23}Na MR. Certainly, the use of ultra-short ^{23}Na MRI TEs (21,24,25,55–58) would avoid the uncertainty in T_2 and minimize the SNR loss from T_2 decay. It would also permit quantitative measurements of TSC. Indeed, the presence of the T_{2f} component not only argues against spin-echo MRI (5,59), but also gradient-refocused echo sequences with TE delays of ≥3 ms (6,46,56). Ultra-short TE ^{23}Na MRI pulse sequences and their associated reconstruction algorithms generally require customized programming that can present a hurdle to clinical studies.

The simplest approach to detecting and imaging the T_{2f} component with ultra-short TE is to eliminate both the slice-selection and phase-encoding gradients with their associated delays, altogether. A three-dimensional (3D) projection reconstruction reminiscent of the original

MRI experiment (60) fits this bill. Such a sequence comprises a short, hard excitation pulse, followed by a constant radial gradient that is reoriented in subsequent applications, to generate a 3D set of angular projections. To optimize the SNR, the projections can be incremented by an angle (111°) related to the "golden ratio" (61,24,27). By this means, TEs as short as 0.2–0.4ms are possible (57,62)–just short enough to catch a few time points of a T_{2f} ~0.5ms signal (Table 2). The constant gradient radial projections *do* over-sample the central low-spatial resolution Fourier components, and under-sample the high spatial frequency components. This is not the most efficient trajectory for covering image *k*-space.

Spiral (25), and "twisted projection imaging" or TPI (56) are alternative *k*-space trajectories that have been used for human cardiac ^{23}Na MRI. Spirals have been used widely in ^{1}H MRI, while the TPI method is responsible for nearly all quantitative measurements of [Na] in humans (63). In TPI, the constant radial projection gradient is replaced by variable spiral-like k-space trajectories that uniformly sample image *k*-space in 3D, as illustrated in Fig. 1(a) (56). Combined with a 400μs hard excitation pulse, TEs of ~400μs are possible, measured to the center of the pulse, since 200μs must still be allowed for turning on the TPI gradient (34,35,56,58).

One significant problem with all sequences using hard pulses, is the effect of RF field (B_1) inhomogeneity. This may arise, for example, when using surface coils for exciting the cardiac ^{23}Na MR signal. The resultant spatially-varying excitation flip-angle (FA) could be addressed by calibrating the spatial B_1 distribution, or by replacing the hard pulse with an adiabatic pulse to provide substantially B_1-independent excitation (21). Presently, the most power-efficient adiabatic pulses are adiabatic half-passage (AHP; FA=90°) pulses whose TE period nominally commences at the end of the pulse (vs. the middle of the hard pulse). Use of AHP thus cuts TE by a further half pulse-length (21). A TPI sequence with AHP excitation is depicted in Fig. 1(b).

Of course, while the T_{2f} signal may be detectable at the start of the acquisition window, it is long gone 2 or 3 T_{2f} periods later, so that the spatial information corresponding to the *k*-space traversed towards the end of the acquisition window–the high spatial frequency components–is still not encoded into the T_{2f} component. Consequently, the image point spread function (PSF) is different for T_{2f} vs. T_{2s} (58), depending on the acquisition parameters (BW, gradient strength, etc). The result can be a blurred ^{23}Na image comprised of a low-resolution T_{2f} image superimposed on a high-resolution T_{2s} image. A comparison of human cardiac images acquired at TEs of 0.4ms and 3.6ms (62) might exemplify such an effect. If spatial resolution is more important than quantifying TSC, setting TE ≥3 ms should eliminate any blurring due to T_{2f}. Fig. 1(c) depicts simulated PSFs for T_{2f} =2 ms and T_{2s} =15ms components excited by a TPI sequence with TE=0.36ms and 12ms readout (58).

For two-dimensional (2D) or restricted 3D ^{23}Na MRI employing slab-selection, the duration of the slice-selection pulse can be cut using truncated selective excitation pulses, achieving TEs as small as 1–1.5ms (24,25). The cost of truncating slice selection is non-uniform slice profiles, which must be accounted for if quantification is the goal.

A final complication for cardiac ^{23}Na MRI pulse sequencing is cardiac motion. In conventional cardiac ^{1}H MRI this is addressed by electro-cardiographic (ECG) gating. If ^{23}Na MRI acquisitions were prospectively gated at a TR equal to the heart-rate, almost the entire SNR advantage of sodium's short T_1 would be lost. Retrospective ECG-gating (24,27) wherein only those frames acquired during active cardiac contraction are omitted, or the acquisition of multiple frames during a timing window limited to a motion-quiet period of say ≤80% of the cardiac cycle (19,20,22,25,55), offer less SNR-costly alternatives. Yet another option is to acquire thousands of projections ungated and bin them into, say, a 10-phase cardiac cine stream (27).

Cardiac ^{23}Na MRI coils

While ^{23}Na MRI can be performed on clinical scanners equipped with broad-band MR transmit/receive capabilities, the limited availability of suitable detection coils and receiver hardware presents another hurdle for patient studies. The usual route after purchasing a ^{23}Na MR channel for the clinical scanner and developing a ^{23}Na MRI pulse sequence capability, is to build (15,21,46) or purchase (20,57) a custom set of ^{23}Na transmit/receive coil systems tailored to the specific application.

The best detectors are those that provide the optimum SNR. From 1.5T to 7T, the ^{23}Na MR frequency ranges from only 16.9 to 79 MHz–a regime ruled by conventional loop detectors. For cardiac ^{23}Na MRI, the choice is invariably surface coils. The diameter of individual surface coils should approximately equal the depth of interest, say 10–15cm for the center of the heart (46). Phased-arrays of surface coils will extend the size of the region of optimum SNR, but require multi-channel ^{23}Na MRI receiver hardware (including preamplifiers, transmit/receive switches, and MR receivers) and phased-array reconstruction, that may or may not be available to the scanner (23,26,46).

Photographs of custom surface and flexible phased-array ^{23}Na MRI coils for human cardiac use at 1.5 T are shown in Fig. 2 (21,22,46). The low ^{23}Na MR frequency at 1.5T necessitates the use of multiple windings and distributed tuning capacitance to achieve the desirable "sample-dominant noise" condition (18). The receiver coils can also be used for MR excitation. Optimized individual surface coils have intrinsically nonuniform B_1s, which must be dealt with for quantitative work (e.g. with the aforementioned AHP pulses; 21). Phased-arrays require either multi-channel excitation (typically unavailable for human cardiac ^{23}Na MRI), or a large separate transmit coil (46). Fig. 3 shows sodium images of the human heart acquired in 4 s and 200 s at 1.5T with the 4-channel cardiac phased-array in Fig. 2, and a separate 40cm surface transmit coil (46).

RF power deposition

Another down-side of ^{23}Na's low gyromagnetic ratio (©) is that it requires 4-times the B_1 for the same FA and duration, yet short pulses are needed to avoid T_{2f} losses. In addition, the RF power deposited in biological tissue, measured as the specific absorption rate, SAR in W/kg, is proportional to $[\upsilon B_1]^2$ (64). Consequently, the SAR for a ^{23}Na study done with the B_1 required to produce the same FA, pulse length, and TR as a ^{1}H MR study at a 4-fold higher MR frequency in the same magnet, is essentially the same, although RF penetration

effects will be less for ^{23}Na due to the lower ^{23}Na RF (64). The benefit of faster scanning due to the short ^{23}Na T_1 may thus be limited in practice by potential RF heating concerns *in vivo*, especially as one moves to higher B_0 in search of higher SNR.

Note also that surface coil excitation has a much greater potential for causing local heating than whole-body excitation due to the presence of high SAR gradients close to the surface coil. In addition, the MRI scanner's inbuilt protections on RF power deposition typically overstate SAR (65). Because the cardiac ^{23}Na coils are likely to be custom-built anyway (Fig. 2), the most prudent course for ensuring safety probably includes testing the coil set for heating using a body phantom of saline gel (23,66).

Quantification

In ^{23}Na MRI signals are quantified as relative changes in signal intensity, or absolute concentration–TSC. Measuring changes in ^{23}Na image intensity is subject to the confounding effects of T_1, T_{2s} and T_{2f} relaxation, nonuniform B_1, and nonuniform detection sensitivity, on reproducibility and the interpretation of any results. Generally, it is prudent to eliminate as many variables as possible (eg, FA variations, T_1 saturation etc.) through experimental design and observing a rigorous protocol. Signal differences can be measured relative to adjacent uninvolved or healthy tissue in a sample region over which sensitivity and/or FA is essentially constant. While such changes cannot be conclusively attributed to changes in TSC, the ^{23}Na MRI signal is often linearly correlated with tissue [Na], for example, as seen in MI (34,46, 67–69).

Absolute TSC at a location (*x, y, z*) can be measured from the ratio of the ^{23}Na image signal intensity $(S^{\text{tissue}}_{x,y,z})$ to that in the same location of a reference phantom of known concentration recorded with the same resolution and FA (21). Saline is a typical concentration reference. In general, the tissue and reference signals require corrections for T_1 saturation and T_2 decay, and for differences in the coil sensitivity (φ) that occur when the coil is loaded with the body vs. the reference phantom. The TSC in the tissue at (*x,y,z*) is given by:

$$[\mathrm{Na}]^{\text{tissue}}_{x,y,z} = \frac{S^{\text{tissue}}_{x,y,z} F^{\text{tissue}}_{x,y,z} E^{\text{tissue}}_{x,y,z} \phi . [\mathrm{Na}]^{\text{ref}}}{S^{\text{ref}}_{x,y,z} F^{\text{ref}} E^{\text{ref}}}. \quad [2]$$

Here, superscripts *tissue* and *ref* denote factors associated with sample and reference acquisitions; and *F* and *E* are the T_1 saturation and T_2 decay correction factors, respectively. The coil loading,φ, can be determined from the ratio of ^{23}Na signals from a small phantom embedded in the coil, recorded during tissue and reference experiments (21). For a TPI or projection sequence employing TE ≤0.4ms, and TR >60ms, the relaxation corrections *E* and *F* approximate unity, so only the signals and loading factors need be measured.

An alternative to measuring TSC that avoids the separate reference acquisition, is to use an external concentration reference in the field-of-view of the ^{23}Na acquisition, at some location, say (x_1, y_1, z_1). Then, although loading is the same, φ must be replaced in Eq. (2) by the ratio, Ψ, of the coil sensitivity at (x_1, y_1, z_1) to that at (x, y, z). Note that except for uniform detectors, $\Psi = \Psi(x_1, y_1, z_1, x, y, z)$ is not a scalar. The reference phantom can also be replaced by an internal reference of known [Na] that changes minimally between subjects.

While the ratio of myocardial to ventricular blood ^{23}Na signals has been reported as a potentially useful semi-quantitative measure (55), extending this to absolute TSC measurements with corrections for differences in spatial sensitivity and relaxation times has yet to be validated.

In the event that FA differs between the reference and tissue acquisitions, or that FA at the tissue differs from its value at the reference location, the signal and F terms in Eq. [2] will be modulated accordingly. In the simple case of TR>>T_1, Eq. [2] is multiplied by the ratio $[\sin\{\alpha(x_1, y_1, z_1)\}/\sin\{\alpha(x, y, z)\}]$, where α is the FA at the two locations. For TR~T_1, the correction would need to be modified further to reflect the FA dependence of the steady-state magnetization of a partial saturation experiment. The potential effects of nonuniform B_1 and partial saturation effects on the accuracy of TSC measurements, are an argument for performing studies at TR>>T_1 with constant FAs provided by separate large excite coils or adiabatic pulses (21,22).

Table 3 summarizes *in vivo* measurements of TSC in chest and heart likely to be encountered in a ^{23}Na MRI study (21, 34, 35, 58, 70–73). Note that cardiac TSC measurements are prone to partial volume errors from voxels close to high-TSC blood (22,50). The canine ^{23}Na MRI measurement of TSC was confirmed by post-mortem atomic absorption spectrophotometry (34).

CLINICAL AND PRE-CLINICAL RESEARCH

Cardiac ^{23}Na MRI is presently limited to patients with chronic MI (19,20,22). The findings are that ^{23}Na MRI shows areas of elevated myocardial signal that correlate with wall-motion abnormalities identified by ^{1}H MRI in 30 subjects studied at 8 days and 6 months post-MI (19). An additional 10 patients studied on days 9, 14, and 90 post-MI revealed a decline in the level of sodium signal elevation from 39%, to 31% to 28% at the three times, respectively, in infarcted vs non-infarcted tissue (20). Another study measuring absolute TSC found 30% elevations in 20 patients with chronic MI measured ≥90 days post-onset (59 ±10 vs 45 ±5 μmol/g in non-MI and 43 ±4μmol/g in controls; 22). This study confirmed that changes in ^{23}Na MR relaxation times were not a confounding factor in the two earlier studies (19,20) that reported changes in sodium signal levels in MI.

Fig. 4 shows TSC levels in normal, MI, and adjacent tissues in the cohort of 20 MI patients, and a ^{23}Na image showing elevated TSC in a patient with a septal MI (22). This study also showed that the magnitude of the TSC increases in MI identified by contrast-enhanced ^{1}H MRI, was unrelated to infarct age or size after 90 days post-onset, or to global ventricular function. An intermediate elevation in TSC was also reported in viable tissue immediately adjacent to the infarction (22). Although intracellular sodium is important for myocellular excitability, TSC measured at rest in these chronic MI patients was not closely associated with an increased risk of arrhythmia, as assessed by electro-physiologic testing for inducibility of monomorphic ventricular tachycardia (22).

The result that sodium ^{23}Na MR levels are elevated in MI is consistent with prior animal work (5,6,67–69). For example, canine studies of acute MI show TSC levels increasing by

up to two-fold or more in the first 8–9 hrs following reperfusion (69). To the extent that the local extracellular sodium pool is buffered at or near 140mM by residual perfusion or diffusion routes, the elevated TSC observed in acute MI as it relates to Eq. [1] is attributable to either: (i) increased $[Na]_{intra}$ due to energetically compromised cellular Na^+/K^+ pump activity; or (ii) an increase in V_{extra} associated with edema, myocyte necrosis or intra-myocardial hemorrhage; or (iii) a combination of both.

Of these, insight on the role of the intracellular component is provided by ^{23}Na MR spectroscopy studies of rodent hearts using shift reagents, which demonstrate huge increases of up to 5-fold in $[Na]_{intra}$ following 30 min of ischemia and dysfunction (74,75). Histochemical measurements suggest that the increase in the V_{intra} factor is, on the other hand, much smaller: up to about 13% in the first hour post-occlusion in isolated canine heart (3,4). On the extracellular side of Eq. [1], microscopic analysis using diffusible markers suggests that about 12–19% of the total myocardial tissue volume in rodents is extracellular (1,67,75), with microscopy evidence that V_{extra} is little-changed in acute reperfused MI (67). Increases in total tissue water content, W, are even more modest: 2–6% increases in reperfused canine MI up to 26 hours post-onset (2,4), or no significant difference from non-MI in acute (57) or chronic MI (49). Thus, these studies in aggregate, point to the bulk of the change in TSC following MI being borne by an increased $[Na]_{intra}$, at least in the acute phase (69).

CONCLUSIONS AND FUTURE

Despite the 6000-fold SNR hit compared to ^{1}H MRI, ^{23}Na is the second most viable nucleus for performing routine human MRI in its natural endogenous form. Yet, cardiac applications remain quite limited. Undoubtedly a declining appetite for supporting non-^{1}H nuclei by the scanner manufacturers has taken a toll: the specialized technical requirements of pulse sequences, detectors and image reconstruction can present insurmountable obstacles for many would-be clinical ^{23}Na MRI researchers. But there are other issues as well. To be useful in a clinical setting, cardiac ^{23}Na MRI needs to add value by providing functional information relating to diagnosis and/or prognosis that is not obtainable by regular ^{1}H MRI or other more convenient means.

Because changes in the tissue ^{23}Na MRI signal primarily reflect changes in intracellular sodium concentration and/or the extracellular volume fraction when the extra-cellular sodium is in homeostasis with the blood pool, ^{23}Na MRI may be particularly sensitive to disorders affecting sodium-potassium pump function, channelopathies (54), as well as injuries or interventions that disrupt the extra-cellular space. Thus, while cardiac applications are presently limited to MI patients, future ^{23}Na MRI studies could reveal altered myocardial TSC associated with sodium pump dysfunction in some cardiomyopthies (7–12). If serum sodium can independently predict outcomes in certain forms of heart failure (11), then TSC measured directly in the heart, might be even more outcome sensitive. Also, just as arm and leg exercise in healthy subjects causes TSC to increase in skeletal muscle (31,70,76)–due to hyperaemia and a net Na^+ influx into the myocytes (1)–it is conceivable that exercise stress could elicit changes in cardiac TSC as well, which might find value in patients with symptoms of myocardial ischemia.

Of course, the potential for false positive detections of altered TSC in the myocardial wall is also high. The adjacent blood pool has twice the sodium; the myocardial wall is relatively thin compared to the spatial resolution of ^{23}Na MRI, and is thinner still in dilated cardiomyopathy and chronic MI; while exercise tends to introduce motion artefacts. All too often, the main competition to ^{23}Na MRI is ^{1}H MRI which, in its many forms–including contrast enhancement, cine, functional tagging, etc.–is already a sensitive, high resolution diagnostic tool for probing cardiac function.

Acknowledgments

The ^{23}Na MRI work in our laboratory was supported by US NIH grants R01 HL61695, the DW Reynolds foundation, and many fruitful collaborations with Ronald Ouwerkerk, Robert G Weiss, and Ray F Li. PAB is supported by the Russell H Morgan Professorship of the Johns Hopkins University Dept. of Radiology and grant 13GRNT17050100 from the American Heart Association.

Abbreviations

TSC	tissue sodium concentration
MI	myocardial infarction
SNR	signal-to-noise ratio
TE	echo-time
BW	bandwidth
FA	flip-angle
TPI	twisted projection imaging
PSF	point spread function
AHP	adiabatic half passage
ECG	electro-cardiographic
T_1	spin, lattice relaxation time
T_2	spin-spin relaxation time
TR	pulse sequence repetition time

References

1. Barclay JA, Harley EJ, Houghton H. Electrolyte content of rat heart atria and ventricles. Circ Res. 1960; 8:1264–1267. [PubMed: 13686881]
2. Jennings RB, Sommers HM, Kaltenbach JP, West JJ. Electrolyte alterations in acute myocardial ischemic injury. Circ Res. 1964; 14:260–264. [PubMed: 14133953]
3. Willerson JT, Scoles F, Mukherjee A, Platt M, Templeton GH, Fink GS, Buja LM. Abnormal myocardial fluid retention as an early manifestation of ischemic injury. Am J Pathol. 1972; 87:159–188. [PubMed: 139829]
4. Whalen DA, Hamilton DG, Ganote CE, Jennings RB. Effect of a transient period of ischemia on myocardial cells I. Effect in cell volume regulation. Am J Pathology. 1974; 74(3):381–397.
5. Cannon PJ, Maudsley AA, Hilal SK, Simon HE, Cassidy F. Sodium nuclear magnetic resonance imaging of myocardial tissue of dogs after coronary artery occlusion and reperfusion. J Am Coll Cardiol. 1986; 7:573–579. [PubMed: 3950237]

6. Kim RJ, Lima JOAC, Chen EL, Reeder SB, Klocke FJ, Zerhouni EA, Judd RM. Fast 23Na magnetic resonance imaging of acute reperfused myocardial infarction: potential to assess myocardial viability. Circulation. 1997; 95:1877–1885. [PubMed: 9107176]
7. Steimle AE, Stevenson LW, Fonarow GC, Hamilton MA, Moriguchi JD. Prediction of improvement in recent onset cardiomyopathy after referral for heart transplantation. J Am Coll Cardiol. 1994; 23(3):553–559. [PubMed: 8113533]
8. Hesse M, Kondo CS, Clark RB, Su L, Allen FL, Geary-Joo CTM, Kunnathu S, Severson DL, Nygren A, Giles WR, Cross JC. Dilated cardiomyopathy is associated with reduced expression of the cardiac sodium channel SCN5aA. Cardiovasc. Res. 2007; 75:498–509. [PubMed: 17512504]
9. Ge J, Sun S, Paajanen V, Wang S, Su C, Yang Z, Li Y, Wang S, Jia J, Wang K, Zou Y, Gao L, Wang K, Fan Z. Molecular and Clinical Characterization of a Novel SCN5A Mutation Associated With Atrioventricular Block and Dilated Cardiomyopathy. Circulation: Arrhythmia and Electrophysiology. 2008; 1:83–92. [PubMed: 19808398]
10. Bezzina CR, Remme CA. Dilated Cardiomyopathy due to Sodium Channel Dysfunction What Is the Connection. Circulation: Arrhythmia and Electrophysiology. 2008; 1:80–82. [PubMed: 19808397]
11. Vilas Boas LGC, Bestetti RB, Otaviano AP, Cardinalli-Neto A, Nogueira PR. Outcome of Chagas cardiomyopathy in comparison to ischemic cardiomyopathy. Internat J Cardiol. 2013; 167:486–490.
12. Coppini R, Ferrantini C, Yao L, Fan P, Del Lungo M, Stillitano F, Sartiani L, Tosi B, Suffredini S, Tesi C, Yacoub M, Olivotto I, Belardinelli L, Poggesi C, Cerbai E, Mugelli A. Late Sodium Current Inhibition Reverses Electromechanical Dysfunction in Human Hypertrophic Cardiomyopathy. Circulation. 2013; 127:575–584. [PubMed: 23271797]
13. Cope FW. Nuclear magnetic resonance evidence for complexing of sodium ions in muscle. Proc Natl Acad Sci U S A. 1965; 54:225–227. [PubMed: 5216356]
14. Delayre JL, Ingwall JS, Malloy C, Fossel ET. Gated sodium-23 nuclear magnetic resonance images of an isolated perfused working rat heart. Science. 1981; 212:935–936. [PubMed: 7233188]
15. Ra JB, Hilal SK, Oh CH, Mun IK. In vivo magnetic resonance imaging of sodium in the human body. Magn Reson Med. 1988; 7:11–22. [PubMed: 3386516]
16. Granot J. Sodium imaging of human body organs and extremities in vivo. Radiology. 1988; 167:547–550. [PubMed: 3357970]
17. Bottomley PA, Hart HR, Edelstein WA, Schenck JF, Smith LS, Leue WM, Mueller OM, Redington RW. Anatomy and metabolism of the normal human brain studied by magnetic resonance at 1.5 Tesla. Radiol. 1984; 150:441–446.
18. Edelstein WA, Glover GH, Hardy CJ, Redington RW. The Intrinsic Signal-to-Noise Ratio in NMR Imaging. Magn Reson Med. 1986; 3:604–618. [PubMed: 3747821]
19. Sandstede JJW, Pabst T, Beer M, Lipke C, Baurle K, Butter F, Harre K, Kenn W, Voelker W, Neubauer S, Hahn D. Assessment of Myocardial Infarction in Humans with 23Na MR Imaging: Comparison with Cine MR Imaging and Delayed Contrast Enhancement. Radiology. 2001; 221:222–228. [PubMed: 11568344]
20. Sandstede JJW, Hillenbrand H, Beer M, Pabst T, Butter F, Machann W, Bauer W, Hahn D, Neubauer S. Time Course of 23Na Signal Intensity After Myocardial Infarction in Humans. Magn Reson Med. 2004; 52:545–551. [PubMed: 15334573]
21. Ouwerkerk R, Weiss RG, Bottomley PA. Measuring Human Cardiac Tissue Sodium Concentrations Measured Using Surface Coils, Adiabatic Excitation and Twisted Projection Imaging With Minimal T2 Losses. J Magn Reson Imag. 2005; 21:546–555.
22. Ouwerkerk R, Bottomley PA, Solaiyappan M, Spooner A, Tomaselli G, Wu KC, Weiss RG. Tissue sodium concentration in myocardial infarction in humans: A quantitative 23Na MR imaging study. Radiology. 2008; 248:88–96. [PubMed: 18566171]
23. AJames, JR.; Lin, C.; Stark, H.; Dale, BM.; Bansal, N. In: Teck Chwee, Lim; Goh, James CH., editors. Optimization and Characterization of Sodium MRI Using 8-channel 23Na and 2-channel 1H RX/TX Coil; 13th International Conference on Biomedical Engineering IFMBE Proceedings; 2009. p. 138-141.http://link.springer.com/chapter/10.1007%2F978-3-540-92841-6_34)

24. Konstandin S, Schad LR. Two-Dimensional Radial Sodium Heart MRI Using Variable-Rate Selective Excitation and Retrospective Electrocardiogram Gating with Golden Angle Increments. Magnetic Resonance in Medicine 70. 2013:791–799.
25. Gai ND, Rochitte C, Nacif MS, Bluemke DA. Optimized Three-Dimensional Sodium Imaging of the Human Heart on a Clinical 3T Scanner. Magnetic Resonance in Medicine. 2014
26. Graess A, Ruehle A, Renz Winter L, Pfeiffer H, Ruff2 J, Rieger J, Niendorf T. Sodium imaging of the heart at 7T: design, evaluation and application of a four-channel transmit/receive surface coil array. J Cardiovasc Magn Reson. 2013; 15(Suppl 1):W14.
27. Resetar A, Hoffmann SH, Graessel A, Waiczies H, Niendorf T, Nagel AM. Retrospectively gated CINE 23Na imaging of the heart at 7.0 T using density-adapted 3D projection reconstruction. Proc. Intl. Soc. Mag. Reson. Med. 2014; 22:436.
28. Cope FW. Spin-echo nuclear magnetic resonance evidence for complexing of sodium ions in muscle, brain, and kidney. Biophys J. 1970; 10:843–858. [PubMed: 5496905]
29. Hubbard PS. Nonexponential nuclear magnetic resonance by quadrupole interactions. J Chem Phys. 1970; 53:985–987.
30. Berendsen HJC, Edzes HT. The observation and general interpretation of sodium magnetic resonance in biological material. Ann N Y Acad Sci. 1973; 204:459–485. [PubMed: 4513164]
31. Rooney W, Springer C. A comprehensive approach to the analysis and interpretation of the resonances of spins 3/2 from living systems. NMR Biomed. 1991; 4:209–226. [PubMed: 1751345]
32. Chang DC, Woessner DE. Spin-echo study of 23 Na relaxation in skeletal muscle: evidence of sodium ion binding inside a biological cell. J Magn Reson. 1978; 30:185–191.
33. Foy BD, Burnstein D. Interstitial sodium nuclear magnetic resonance relaxation times in perfused hearts. Biophys J. 1990; 58:127–134. [PubMed: 2383627]
34. Constantinides CD, Kraitchman DL, O'Brien K, Boada FE, Gillen J, Bottomley PA. Noninvasive quantification of total sodium concentrations in acute reperfused myocardial infarction using 23Na MRI. Magn Reson Med. 2001; 46:1144–1151. [PubMed: 11746581]
35. Constantinides C, Gillen JS, Boada FE, Pomper MG, Bottomley PA. Human skeletal muscle: 23Na MR imaging and quantification-potential applications in exercise and disease. Radiology. 2000; 216:559–568. [PubMed: 10924586]
36. Pabst T, Sandstede J, Beer M, Kenn W, Neubauer S, Hahn D. Sodium T2* relaxation times in human heart muscle. J Magn Reson Imaging. 2002; 15:215–218. [PubMed: 11836780]
37. Pabst T, Sandstede J, Beer M, Kenn W, Neubauer S, Hahn D. Evaluation of sodium T1 relaxation times in human heart. J Magn Reson Imaging. 2003; 17:726–729. [PubMed: 12766903]
38. Pettegrew JW, Woessner DE, Minshew NJ, Glonek T. Sodium-23 NMR analysis of human whole blood, erythrocytes, and plasma: chemical shift, spin relaxation and intracellular sodium concentration studies. J Magn Reson. 1984; 57:185–196.
39. Perman WH, Turski PA, Houston LW, Glover GH, Hayes CE. Methodology of in vivo human sodium MR imaging at 1.5 T. Radiology. 1986; 160:811–820. [PubMed: 3737922]
40. Shinar H, Navon G. Sodium-23 NMR relaxation times in body fluids. Magn Reson Med. 1986; 3:927–934. [PubMed: 3821467]
41. Winkler SS, Thomasson DM, Sherwood K, Perman WH. Regional T2 and sodium concentration estimates in the normal brain by sodium-23 MR imaging at 1.5T. J Comput Assist Tomogr. 1989; 13:561–566. [PubMed: 2745773]
42. Perman, WH.; Turski, PA. Biomedical magnetic resonance imaging: principles, methodology and applications. New York, NY: VCH; 1984. p. 421-468.
43. Buist JR, Deslauriers R, Saunders JK, Mainwood GW. 23Na and flame photometric studies of the NMR visibility of sodium in rat muscle. Can J Physiol Pharmacol. 1991; 69:1663–1669. [PubMed: 1804513]
44. Kushnir T, Knubovet T, Itzchak Y, Eliav U, Sadeh M, Rapoport L, Kott E, Navon G. In vivo 23Na NMR studies of myotonic dystrophy. Magn Reson Med. 1997; 37:192–196. [PubMed: 9001142]
45. Kemp-Harper R, Styles P, Wimperis S. Measurement of 23Na transverse relaxation in vivo: the flip-angle-independent experiment. J Magn Reson Ser B. 1995; 109:223–228.

46. Lee RF, Giaquinto R, Constantinides, Souza S, Weiss RG, Bottomley PA. A broadband phased-array system for direct phosphorus and sodium metabolic MRI on a clinical scanner. Magn Reson Med. 2000; 43:269–277. [PubMed: 10680691]
47. Snyder, WS.; Cook, MJ.; Nasset, ES.; Karhausen, LR.; Howells, GP.; Tipton, IH. Re- port of the task group on reference man: International Commission on Radiological Protection No. 23. Oxford, England: Pergamon Press; 1984. p. 26-32.214–215, 280–285, 196
48. Polimeni PI. Extracellular space and ionic distribution in the rat ventricle. Am J Physiol. 1974; 227:676–683. [PubMed: 4413398]
49. Bottomley PA, Weiss RG. Noninvasive magnetic resonance detection of creatine depletion in non-viable infarcted myocardium. Lancet. 1998; 351:714–718. [PubMed: 9504516]
50. Judd RM, Resar JR, Yin FC. Rapid measurements of diastolic intra-myocardial vascular volume. Am J Physiol. 1993; 265:H1038–H1047. [PubMed: 8238391]
51. Constantinides CD, Rogers J, Herzka D, Bolar D, Boada FE, Kraitchman DL, Bottomley PA. Superparamagnetic iron oxide MION as a potential contrast agent for 23Na MRI in myocardial infarction. Magn Reson Med. 2001; 46:1164–1168. [PubMed: 11746583]
52. van Emous JF, van Echteld CJA. Changes of intracellular sodium T2 relaxation times during ischemia and reperfusion in isolated rat hearts. Magn Reson Med. 1998; 40:679–683. [PubMed: 9797149]
53. Narayana, PA.; Kulkarni, MV.; Mehta, SD. NMR of 23Na in biological systems. In: Partain, CL.; Price, RR.; Patton, JA.; Kulkarni, MV.; Everette, JA., Jr, editors. Magnetic resonance imaging. 2nd. Vol. 2. Philadelphia, Pa: Saunders: physical principles and instrumentation; 1998. p. 1553-1563.
54. Weber MA, Nielles-Vallespin S, Huttner HB, Wohrle JC, Jurkat-Rott K, Lehmann-Horn F, Schad LR, Kauczor HU, Essig M, Meinck HM. Evaluation of Patients with Paramyotonia at 23Na MR Imaging during Cold-induced Weakness. Radiol. 2006; 240:489–500.
55. Pabst T, Sandstede J, Beer M, Kenn W, Greiser A, von Kienlin M, Neubauer S, Hahn D. Optimization of ECG-triggered 3D 23Na MRI of the human heart. Magn Reson Med. 2001; 45:164–166. [PubMed: 11146499]
56. Boada FE, Gillen JS, Shen GX, Chang SY, Thulborn KR. Fast three dimensional sodium imaging. Magn Reson Med. 1997; 37:706–715. [PubMed: 9126944]
57. Nielles-Vallespin S, Weber MA, Bock M, Bongers A, Speier P, Combs SE, Wohrle J, Lehmann-Horn F, Essig M, Schad LR. 3D radial projection technique with ultrashort echo times for sodium MRI: Clinical applications in human brain and skeletal muscle. Magn Reson Med. 2007; 57:74–81. [PubMed: 17191248]
58. Lu A, Atkinson IC, Claiborne TC, Damen FC, Thulborn KR. Quantitative Sodium Imaging With a Flexible Twisted Projection Pulse Sequence. Magn Reson Med. 63:1583–1593. 2010. [PubMed: 20512862]
59. Ra JR, Hilal SK, Cho ZH. A method for in vivo MR imaging of the short T2 component of sodium-23. Magn Reson Med. 1986; 3:296–302. [PubMed: 3713493]
60. Lauterbur PC. Image Formation by Induced Local Interactions: Examples Employing Nuclear Magnetic Resonance. Nature. 1973; 242:190–191.
61. Winkelmann S, Schaeffter T, Koehler T, Eggers H, Doessel O. An Optimal Radial Profile Order Based on the Golden Ratio for Time-Resolved MRI. IEEE Trans Med Im. 2007; 26:68–76.
62. Jerecic R, Bock M, Wacker C, Bauer W, Schad LR. 23Na-MRI of the human heart using a 3D radial projection technique. Biomed Tech. 2002; 47(Suppl 1/1):458–459.
63. Bottomley, PA. Sodium MRI in Man: Technique Findings. In: Harris, RK.; Wasylishen, RE., editors. Encyclopedia of Magnetic Resonance. John Wiley: Chichester; 2012. eMagRes, Vol 1: 353–366. DOI 10.1002/9780470034590.emrstm1252
64. Bottomley PA, Andrew ER. RF magnetic field penetration, phase-shift and power dissipation in biological tissue: Implications for NMR imaging. Phys Med Biol. 1978; 23:630–643. [PubMed: 704667]
65. El-Sharkawy AEM, Qian D, Bottomley PA, Edelstein WA. A Multichannel, Real-Time MRI RF Power Monitor for Independent SAR Determination. Med Phys. 2012; 39:2334–2341. [PubMed: 22559603]

66. El-Sharkawy AEM, Gabr RE, Schär M, Weiss RG, Bottomley PA. Quantification of human high-energy phosphate metabolite concentrations at 3T with partial volume and sensitivity corrections. NMR Biomed. 2013; 26:1363–1371. [PubMed: 23729378]

67. Kim RJ, Judd RM, Chen EL, Fieno DS, Parish TB, Lima JAC. Relationship of elevated 23Na magnetic resonance image intensity to infarct size after acute reperfused myocardial infarction. Circulation. 1999; 100:185–192. [PubMed: 10402449]

68. Constantinides C, Weiss RG, Lee R, Bolar D, Bottomley PA. Restoration of low resolution metabolic images with a priori anatomic information: 23Na MRI in myocardial infarction. Magn Reson Imaging. 2000; 18:461–471. [PubMed: 10788724]

69. Rochitte CE, Kim RJ, Hillenbrand HB, Chen EL, Lima JAC. Microvascular integrity and the time course of myocardial sodium accumulation after acute infarction. Circ Res. 2000; 87:648–655. [PubMed: 11029399]

70. Bansal N, Szczepaniak L, Ternullo D, Fleckenstein JL, Malloy CR. Effect of exercise on 23Na MRI and relaxation characteristics of the human muscle. J Magn Reson Imag. 2000; 11:532–538.

71. Jacobs MA, Ouwerkerk R, Wolff AC, Stearns V, Bottomley PA, Barker PB, Argani P, Khouri N, Davidson NE, Bhujwalla Z, Bluemke DA. Multiparametric and multinuclear magnetic resonance imaging of human breast cancer: current applications. Technology in Cancer Research & Treatment. 2004; 3:543–550. [PubMed: 15560711]

72. Ouwerkerk R, Jacobs MA, Macura KJ, Wolff AC, Stearns V, Mezban SD, Khouri NF, Bluemke DA, Bottomley PA. Elevated Tissue Sodium Concentration in Malignant Breast Lesions Detected With Noninvasive 23Na MRI. Breast Cancer Research and Treatment. 2007; 106:151–160. [PubMed: 17260093]

73. Meike Danisch M, Kalayciyan R, Wetterling F, Schad LR. Bilaterale 23Na-MR-Bildgebung der Mamma und Quantifizierung der Natriumkonzentration. Z. Med. Phys. 2014; 14:65–72. [PubMed: 23969091]

74. Malloy CR, Buster DC, Castro MMCA, Geraldes CFGC, Jeffrey FMH, Sherry AD. Influence of global ischemia on intracellular sodium in the perfused rat heart. Magn Reson Med. 1990; 15:33–44. [PubMed: 2374498]

75. van Echteld JA, Kirkels JH, Eijgelshoven MHJ, van der Meer P, Ruigrok TJC. Intracellular sodium during ischemia and calcium-free perfusion: a 23Na NMR study. J Mol Cell Cardiol. 1991; 23:297–307. [PubMed: 1880814]

76. Ouwerkerk R, Lee RF, Bottomley PA. Dynamic changes in sodium levels in human exercising muscle measured with 23Na MRI. Proc Intl Soc Mag Reson Med. 1999; 3:1530.

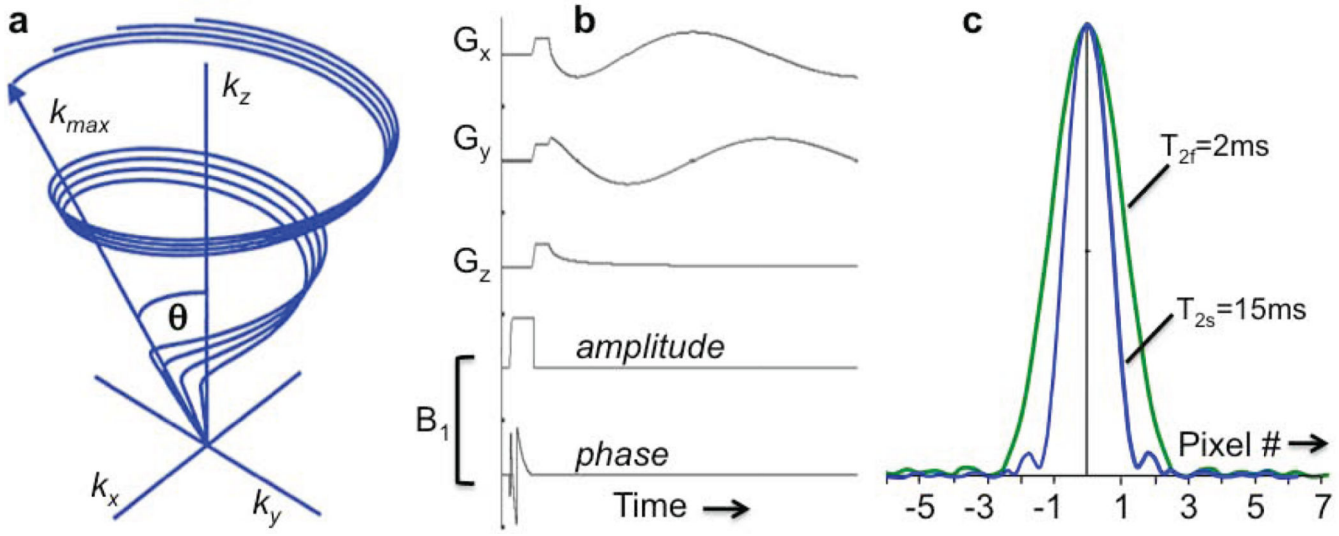

Figure 1.

(a) Partial *k*-space sampling scheme for twisted projection imaging (TPI). The maximum *k* forms a sphere of radius k_{max}, and the projections lie on a surface of a cone whose twist is adjusted to maintain critical sample density (56). (b) The TPI pulse sequence with adiabatic half passage excitation. The hard pulse of the original TPI sequence (56) is replaced by an amplitude (amp.) and phase modulated AHP pulse, but the gradient waveforms, G_x, G_y, and G_z, are the same, and depicted for one of the projections (21). (c) Simulated point spread function for T_{2f} =2ms and T_{2s} =15ms signal components excited by a TPI sequence with TE=0.36ms, a 31.3 kHz bandwidth, 12 ms readout, 22cm FOV, 44×44×44 array size, and Δx =5mm nominal isotropic spatial resolution (58). The T_{2s} component has a full-width at half-maximum (fwhm) of about 1.5Δx (7.5 mm), while the fwhm of the T_{2f} component is 2.4Δx (12.0 mm). (Adapted from Refs. 21,56, 58).

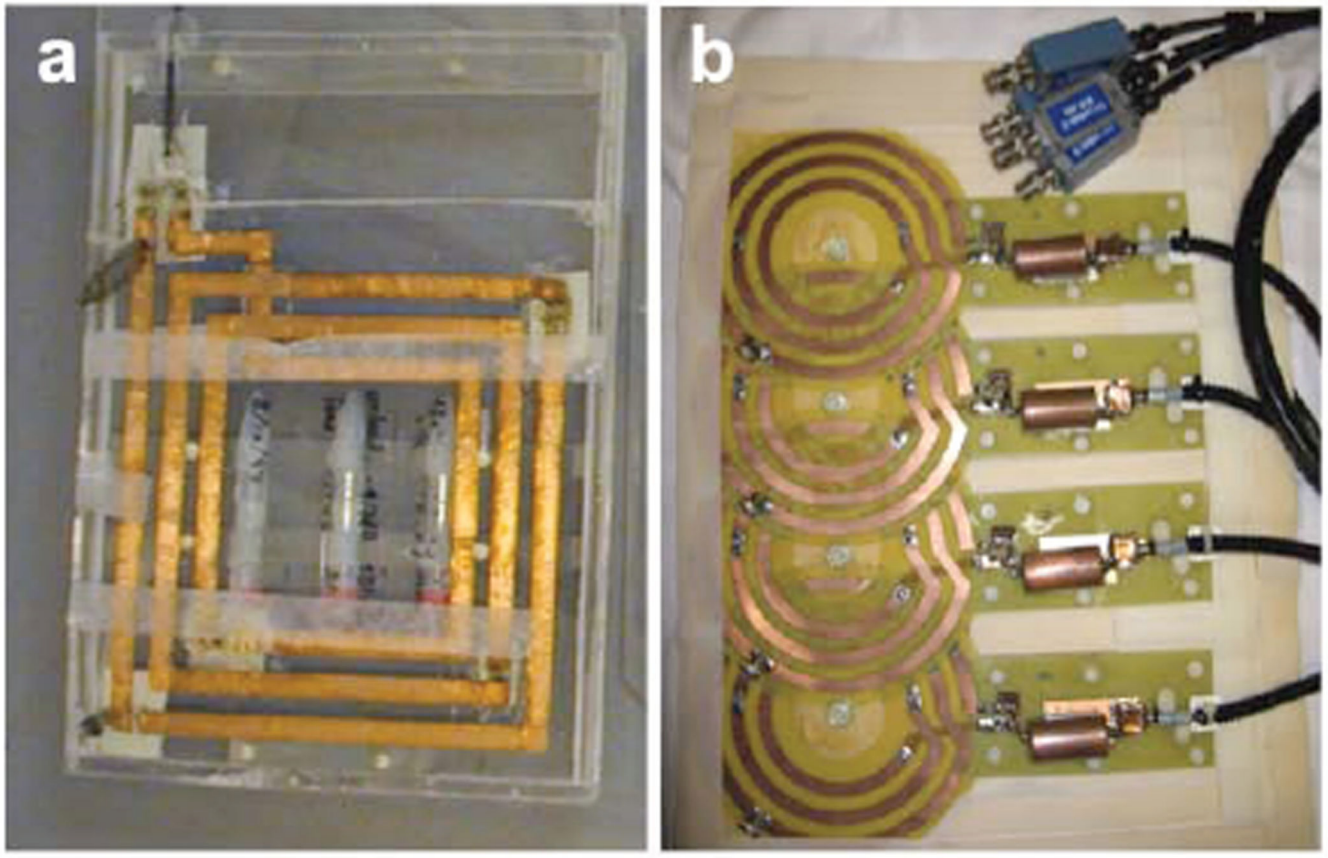

Figure 2.

Custom-built coils for human cardiac ^{23}Na MRI at 1.5 Tesla (16.9 MHz). (a) Square 25×25 cm three-turn transmit/receive surface coil used for quantitative cardiac TSC studies employing adiabatic excitation (21). The coil has 3 embedded vials of saline gel to serve as sensitivity references, and a mount permitting exchange with a conventional cardiac ^{1}H coil for cardiac MRI (21,22). (b) A 4-channel ^{23}Na phased-array constructed from 15-cm, 3-turns coils for increased inductance at the lower ^{23}Na frequency (46). The detectors were fabricated on 0.25-mm thick flexible printed circuit board, with a separate 40-cm square single-turn transmit coil for excitation.

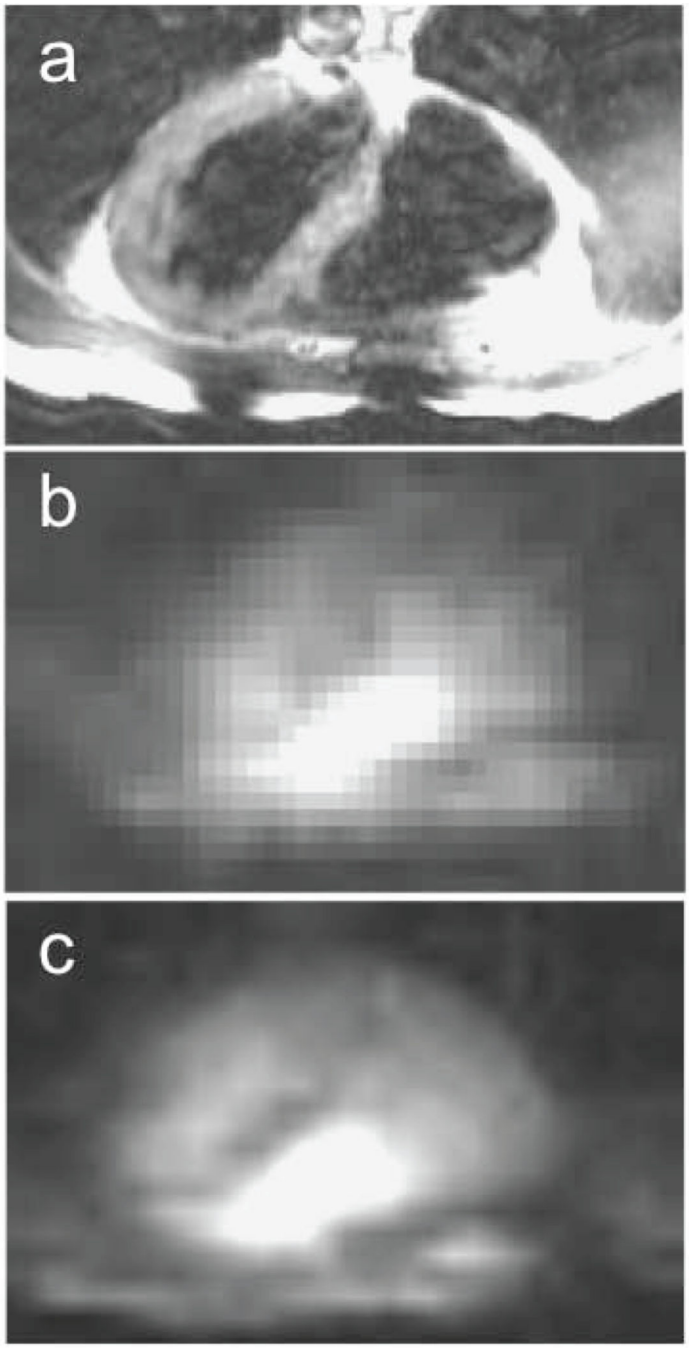

Figure 3.

(a) Conventional ^{1}H trans-axial image, and (b) corresponding single slice ^{23}Na MRI of the human heart acquired with the phased-array in Fig. 2(b) using a slice-selective gradient refocused echo (GRE) sequence in 4s, and (c) 200s (array size, 32 × 32; resolution, 1 × 1 × 4 cm^{3}; TR/TE= 33/5 ms; from Ref. 46).

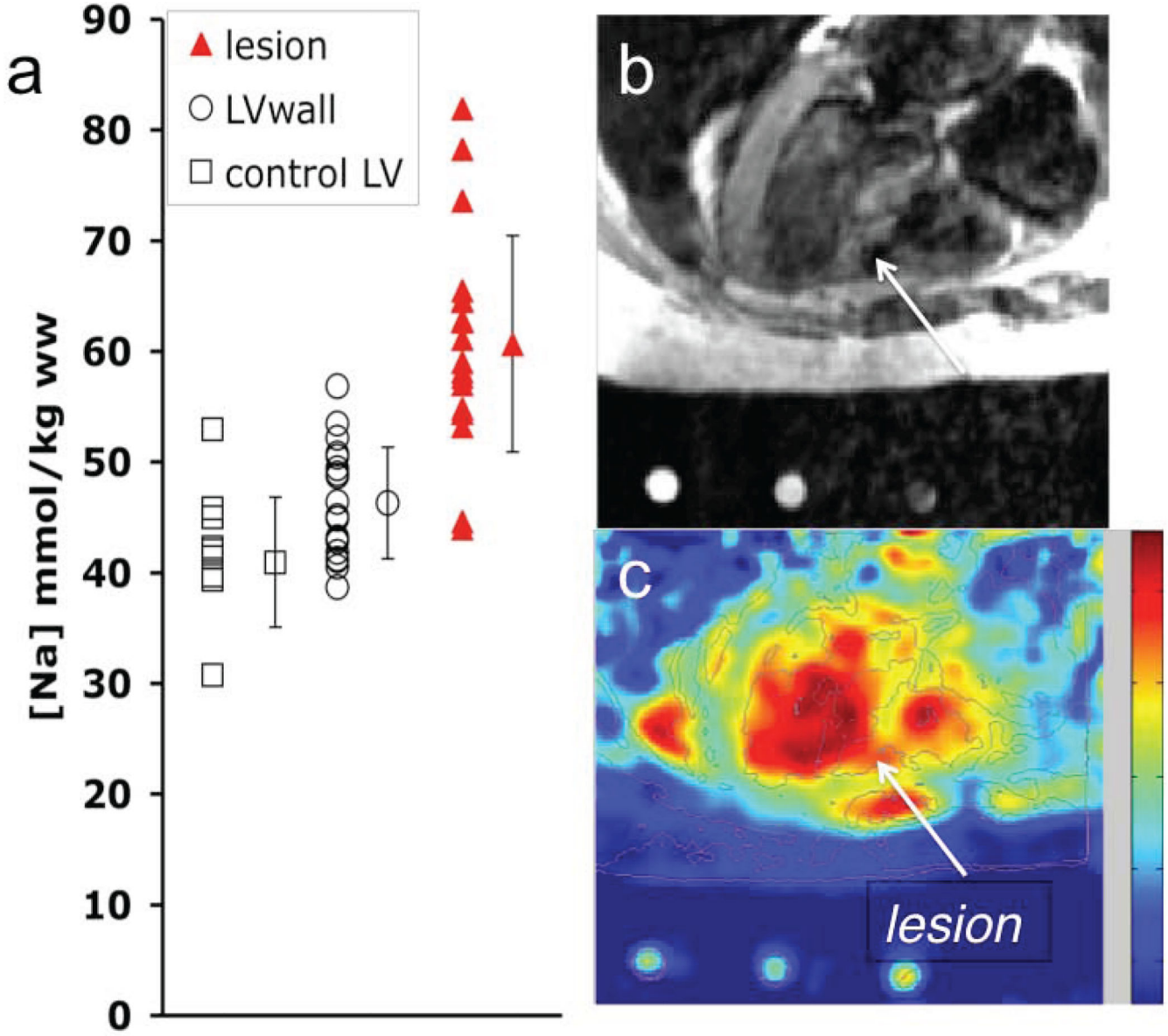

Figure 4.

(a) TSC values in infarcted and remote myocardium in 20 MI patients, and in adjacent tissue in 11 of the patients. Vertical bars denote means ±SD. TSC is significantly increased in MI vs remote tissue (P <0.001). (b) Trans-axial gated ^{1}H fast spin-echo image, and (c) corresponding ^{23}Na image from a 3D TPI data set (TR/TE=85/0.4 ms; isotropic spatial resolution =6 mm) from a 61-year-old man with a remote septal MI (arrow). Color scale is proportional to TSC and includes B_1 correction; LV=left ventricle. (Adapted from Ref. 22).

Table 1

NMR properties and predicted sensitivity of ^{23}Na MRI in tissue relative to ^{1}H.

	^{1}H MRI in tissue	**^{23}Na MRI in tissue**
Magnetic moment (in nuclear magnetons)	2.7927	2.2161
Spin quantum number	1/2	3/2
NMR frequency @ 1 Tesla	42.577	11.262
Sensitivity* @ constant field per nucleus $\propto \upsilon^3 I(I+1)$	1	0.0925
Relative SNR at constant B_0/nucleus*	1	0.35
In vivo concentration (mol/kg)	42.8	0.04
In vivo conc. of nucleus (mol/kg)	85.6	0.04
SNR of moiety in tissue	85.6	0.014
SNR relative to 1H of tissue water†	1	1.64×10^{-4}

*υ =NMR frequency,

I =nuclear spin quantum number.

†Assumes SNR $\propto \upsilon^1$.

Table 2

Some reported T_1 and T_2 relaxation times for ^{23}Na in intact muscle, heart and blood.

Tissue/Sample	T_1(ms) [a]	T_{2f} (ms) [a]	T_{2s} (ms) [a]	B_o (T)	Ref
Blood plasma (human)	30 ±1		17 ±1	4.7	38
Blood plasma		12	49.5	1.5	39
Blood plasma	37.3 ±1.0		24.5 ±0.8	8.5	40
Blood, human *in vivo*			20.9 ±6.0	1.5	41
Blood, human	30.8 ±1.3	3.25 ±0.29	18.1 ±1.3	1.5	35
Blood, human LV, *in vivo*	31.1 ±7.5		19.3 ±3.3	1.5	36,37
Blood, human heart	31.9±4.1		20.1 ±1.3	3T	24
Red blood cells	30.1 ±3.1	4.3 ±1.2	19.9 ±1.8	1.5	35
Red blood cells	30 ±3		14 ±3	4.7	38
Red blood cells		6.3	27.2, 17.3[b]	1.5	42
Rat muscle	18.3 ±0.5	1.59 ±0.16	16.1 ±2.6	2.3	32
Rat muscle	12 ±1		15 ±8	0.89	28
Rat muscle hindlimb		3–4	21–37	7.05	43
Human skeletal muscle		1.2 ±0.2	32.5 ±8.2	1.91	44
Human skeletal muscle		0.6–2.5	21.2–23.1	2	45
Human skeletal muscle	32.3 ±0.5	0.46 ±0.21	12.3 ±1.9	1.5	35
Canine heart-viable tissue	34.2 ±0.9	3.6 ±0.6[c]	31.5 ±0.8	4.7	6
-non-viable	26.2 ±1.5	2.2 ±0.2 [c]	21.9 ±1.2	4.7	6
Canine heart-normal		2.44 ±0.4	15.2 ±1.8[d]	1.5	34
-infarcted		2.04 ±0.2	22.7 ±3.4[d]	1.5	34
Human heart	31.6±7.0		13.3±4.3	1.5	36,37
Human heart	19.9±6.2		12.4±1.8	3	24

[a] Values are mean±SD. Empty cells: values not determined or not reported

[b] Composite T_{2s} relaxation reported.

[c] Significant decrease in non-viable vs. viable tissue

[d] Significant elevation in infarcted vs. normal state (p <0.004)

Table 3

Some *in vivo* ^{23}Na MRI measurements of total sodium content in normal tissue.

Tissue	n	[Na] mmol/kg wet wt	Ref.	MRI method
Human skeletal muscle	10	28.4 ±3.6	35	TPI
	5	26.2 ±3.3	58	TPI
	5	26 ±4	70	3DGRE
Canine heart	6	34.4 ±2.8	34	TPI
Human heart	10	43 ±4	21	TPI
Human adipose tissue	10	17 ±4	21	TPI
		20 ±2	71	TPI
Human ventricular blood	10	79 ±8	21	TPI
Human breast, fibrous	9	28 ro	71	TPI
	19	33 rou[a]	72	TPI
	2	57 ±14	73	3DDR

Values are mean ±SD; TPI=twisted projection imaging; 3DGRE=three-dimensional (3D) gradient refocused echo; 3DDR=3D density-adapted radial acquisition.

[a]Converted from mmoles/liter of wet tissue assuming a specific gravity of 1.04 (46).